

Photoacoustic flow cytometry: principle and application for real-time detection of circulating single nanoparticles, pathogens, and contrast dyes *in vivo*

Vladimir P. Zharov

University of Arkansas for Medical Sciences
Phillips Classic Laser Laboratories
Little Rock, Arkansas 72205
E-mail: ZharovVladimirP@uams.edu

Ekaterina I. Galanzha

University of Arkansas for Medical Sciences
Phillips Classic Laser Laboratories
Little Rock, Arkansas 72205
and
Saratov State University
Institute of Optics and Biophotonics
Saratov 410012, Russia

Evgeny V. Shashkov

University of Arkansas for Medical Sciences
Phillips Classic Laser Laboratories
Little Rock, Arkansas 72205
and
Prokhorov General Physics Institute
Moscow 119991, Russia

Jin-Woo Kim

University of Arkansas
Department of Biological and Agricultural
Engineering
Fayetteville, Arkansas 72701

Nikolai G. Khlebtsov

Institute of Biochemistry and Physiology of Plants
and Microorganisms
Saratov 410049, Russia

Valery V. Tuchin

Saratov State University
Institute of Optics and Biophotonics
Saratov 410012, Russia

1 Introduction

Flow cytometry (FC) is a well-established diagnostic method that revolutionized cell diagnostics *in vitro*.^{1–3} In this technique, cells are introduced into an artificial flow, and laser-induced scattering and/or fluorescent light from them are detected with photodetectors. Modern multicolor FCs with advanced fluorescent probes are widely used in basic and clinical research, providing rapid analysis of large populations of cells, detection of rare cancer cells, and evaluation of cell

Abstract. The goal of this work is to develop *in vivo* photoacoustic (PA) flow cytometry (PAFC) for time-resolved detection of circulating absorbing objects, either without labeling or with nanoparticles as PA labels. This study represents the first attempt, to our knowledge, to demonstrate the capability of PAFC with tunable near-infrared (NIR) pulse lasers for real-time monitoring of gold nanorods, *Staphylococcus aureus* and *Escherichia coli* labeled with carbon nanotubes (CNTs), and contrast dye Lymphazurin in the microvessels of mouse and rat ears and mesenteries. PAFC shows the unprecedented threshold sensitivity *in vivo* as one gold nanoparticle in the irradiated volume and as one bacterium in the background of 10^8 of normal blood cells. The CNTs are demonstrated to serve as excellent new NIR high-PA contrast agents. Fast Lymphazurin diffusion in live tissue is observed with rapid blue coloring of a whole animal body. The enhancement of the thermal and acoustic effects is obtained with clustered, multilayer, and exploded nanoparticles. This novel combination of PA microscopy/spectroscopy and flow cytometry may be considered as a new powerful tool in biological research with the potential of quick translation to humans, providing ultrasensitive diagnostics of pathogens (e.g., bacteria, viruses, fungi, protozoa, parasites, helminthes), metastatic, infected, inflamed, stem, and dendritic cells, and pharmacokinetics of drug, liposomes, and nanoparticles in deep vessels (with focused transducers) among other potential applications. © 2007 Society of Photo-Optical Instrumentation Engineers. [DOI: 10.1117/1.2793746]

Keywords: *in vivo* flow cytometry; photoacoustic spectroscopy; microscopy; small animals; blood circulation; gold nanorods; carbon nanotubes; Lymphazurin; bacteria.

Paper 07105SSRR received Mar. 19, 2007; revised manuscript received May 28, 2007; accepted for publication Jun. 11, 2007; published online Oct. 24, 2007.

viability and drug–cell interactions, among many other applications.^{1,2} Nevertheless, the technique requires invasive extraction of cells from a living organism and associated procedures (e.g., fluorescence labeling and sorting), which may lead to unpredictable artifacts (e.g., cytotoxicity) and prevent long-term cell monitoring in the native biological environment for early diagnosis (and hence, well-timed prevention) of metastasis, inflammations, sepsis, immunodeficiency disorders, stroke, or heart attack.^{1,4,5} Besides, powerful fluorescent labeling used in most FCs *in vitro*^{1,2} and recently FC *in vivo*,⁶ despite significant progress in the development of new fluorescent probes (e.g., quantum dots),⁷ is still subject to pho-

Address all correspondence to Ekaterina Galanzha, Phillips Classic Laser Laboratories, University of Arkansas for Medical Sciences, 4301 West Markham St. #543, Little Rock, AR 72205; Tel: 501–526–7620; Fax: 501–686–8029; E-mail:EGalanzha@uams.edu

tobleaching, blinking, or cytotoxicity, which may prevent extending FC capability to *in vivo* study, at least on humans. Moreover, growing evidences show that fluorescence labeling may seriously distort genuine cell properties and cellular physiologic function.^{8–13} For example, traditional fluorescent dyes for leukocytes, such as acridine orange and rhodamine 6G, are mutagenic and carcinogenic, as well as possibly causing phototoxic effects.^{8–10} Fluorescence imaging of microvessels with conventional fluorescein isothiocyanate–dextran (FITC) dye leads to elevated interstitial pressure and altered plasma viscosity.¹³ These findings may raise some concern of the actual rate estimation of the cell elimination from the circulation, which can be caused by native properties of apoptotic and cancer cells and/or the significant influence of the fluorescent tags. All these problems gain importance in *in vivo* human studies and emphasize the need for alternative approaches that do not need conventional fluorescence labeling.

In 2004, we described the first *in vivo* flow cytometer with photothermal (PT) detection of circulating cells that are not sensitive to light scattering and do not require cell labeling, or can be used with new nontoxic PT labels with high efficiency transformation of absorbed energy in heat and accompanied acoustic effects.^{14–18} In this technique, the cells in blood or lymph flow are irradiated with several laser beams of different wavelengths; then, laser-induced PT effects on the individual cells are detected with corresponding schematics. In particular, the setup provides cell irradiation in pulse and continuous-wave (cw) modes using: 1. first pulse (8-ns width) with tunable wavelength in the range of 420 to 2300 nm; 2. second pulse (12-ns width) with a fixed wavelength of 639 nm and tunable time delay up to 5 μ s relative to the first pulse; and 3. cw radiation at 633 nm from a He–Ne laser. As in conventional absorption spectroscopy, the basic information provided by PT-based techniques, including photoacoustic (PA) and thermolens methods, involves absorption,^{19,20} which is used as intrinsic cell signature. For nonfluorescent samples, PT methods currently offer the highest sensitivity for absorption (e.g., 10^{-2} to 10^{-3} cm⁻¹ at single cell level), which is at least 4, if not 5, orders of magnitude better than that of absorption spectroscopy. This enables noninvasive (a short-term temperature elevation <1 to 5 °C) detection of a single, unlabeled cell having specific absorption spectra in the visible and especially, near-infrared (NIR) spectral ranges that are unachievable with other existing methods.²¹

Recently, we demonstrated that the PA technique, which has been widely used to study many cells in irradiated volume only,²² can be extended to the analysis of single cells *in vitro* as well as *in vivo*.^{23–28} In this new application, the PA technique demonstrated unprecedented sensitivity threshold *in vivo* as one cancer cell in the background of 10^8 normal cells in the blood flow.²⁷ The developed setup with several tunable spectral channels has the potential to detect and spectrally identify cells (PA spectroscopy *in vivo*) simultaneously in different vessels by allowing us to label cells with NIR multi-color PT/PA probes, including conventional contrast dyes such as indocyanine green (ICG) dye²⁷ and advanced gold nanoparticles such as strongly absorbing gold nanorods with absorption maximum at different wavelengths.^{27,28} Tunable NIR pulse lasers are ideally suited for sensing individual cells in relatively deep blood vessels because of the minimal ab-

sorption of most biotissues in this spectral range⁵ and the possibility to use fiber²⁸ or catheter-based light delivery¹⁶ in combination with focused ultrasound transducers and time-resolved detection techniques.

In the present study, we demonstrate for the first time, to the best of our knowledge, the applicability of the innovative PA flow cytometry (PAFC) for real-time, quantitative monitoring in the blood circulation of individual gold nanoparticles such as gold nanorods (GNRs), bacteria such as *Staphylococcus aureus* and *Escherichia coli* labeled with the ICG dye and carbon nanotubes (CNTs), and conventional contrast agents, such as Lymphazurin.

2 Methods and Materials

2.1 *In Vivo* Flow Cytometry with Photoacoustic Schematics

In PAFC, laser-induced PA waves (referred to as PA signals) from the cells in the blood (or lymph) flow are detected with an ultrasound transducer attached to the skin (Fig. 1). The PAFC system was built on the platform of an Olympus BX51 microscope (Olympus America, Inc. Center Valley, Pennsylvania) and a tunable optical parametric oscillator (OPO) pumped by a Nd:YAG laser (both from Lotis Limited, Minsk, Belarus). Laser pulses had an 8-ns pulse width, a regular repetition rate of 10 Hz with ability to provide short-term 50 Hz, and a wavelength in the range of 420 to 2300 nm (Fig. 2). Laser energy was delivered to vessels with conventional lenses, or fibers.²⁸ PA signals from the ultrasound transducers (unfocused XMS-310, Panametrics, 10 MHz, (Olympus NTD Inc., Waltham, Massachusetts); focused cylindrical V316-SM, Panametrics, 20 MHz, focused lengths of 6.5 and 25 mm; and customized resonance transducers) and amplifier (models 5662 and 5678, Panametrics, bandwidth 50 kHz to 5 and 40 MHz customized amplifiers with adjustable high and low frequency boundary in the range of 50 to 200 KHz and 1 to 20 MHz, respectively; resonance bandwidth of 0.3 to 1 MHz) were recorded with a boxcar (Stanford Research Systems, Inc., Sunnyvale, California) and a Tektronix TDS 3032B oscilloscope, and were analyzed with standard and customized software. The boxcar technique provided averaging PA signals from cells in the blood vessels and time-resolved discrimination from background signals from surrounding tissue because of the different time delays. The signals from the oscilloscope screen were also recorded with a digital camera (Sony Corporation of America, New York, NY) and video camera (JVC Company of America, Wayne, New Jersey).

Because PAFC is a relatively new tool in biological cell study, it was integrated with well-established PT flow cytometry (PTFC) (Fig. 2)^{14–18} to validate PAFC parameters. In particular, in the thermolens mode of PTFC, laser-induced temperature-dependent refractive heterogeneity around cellular endogenous absorbing structures (or contrast agents) cause defocusing of a colinear He–Ne laser probe beam (model 117A 633 nm, 1.4 mW; Spectra-Physics, Inc., Mountain View, California), and a subsequent reduction in the beam's intensity at its center, which is detected with a photodiode (C5658; Hamamatsu Corp., Hamamatsu City, Japan) with a 0.5-mm-diameter pinhole as an integrated PT response from a whole cell.

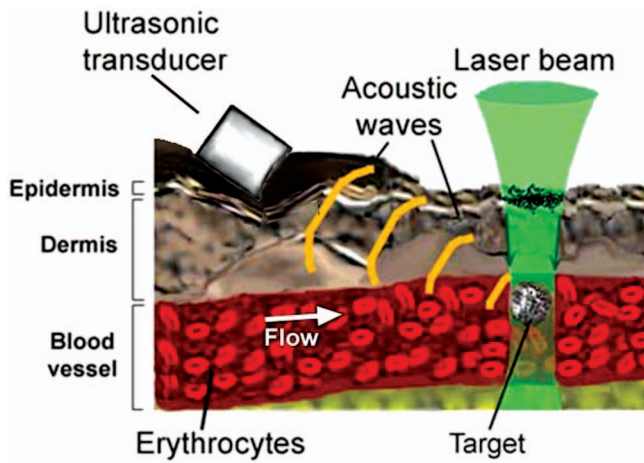


Fig. 1 Principle of PA detection of single absorbing targets in blood flow *in vivo*.

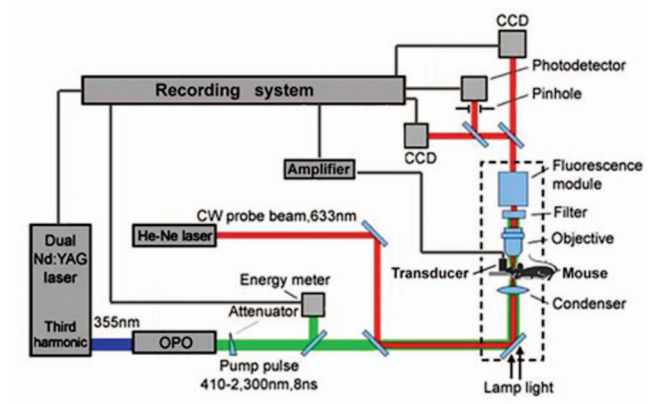


Fig. 2 Schematic of the integrated PA/PT flow cytometry.

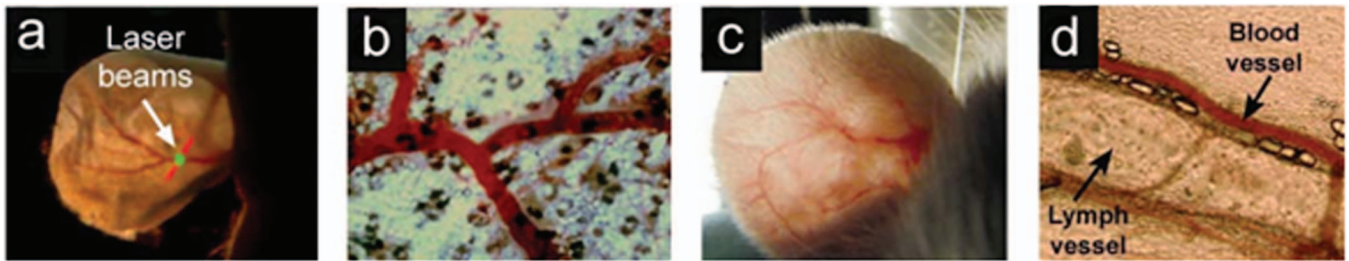


Fig. 3 (a) Mouse ear photograph with the linear probe laser beam (red) and circular pump laser beam (green). (b) Mouse ear blood microvessels at 10 \times magnification. (c) Rat ear blood microvessels. (d) Rat mesenteric structures.

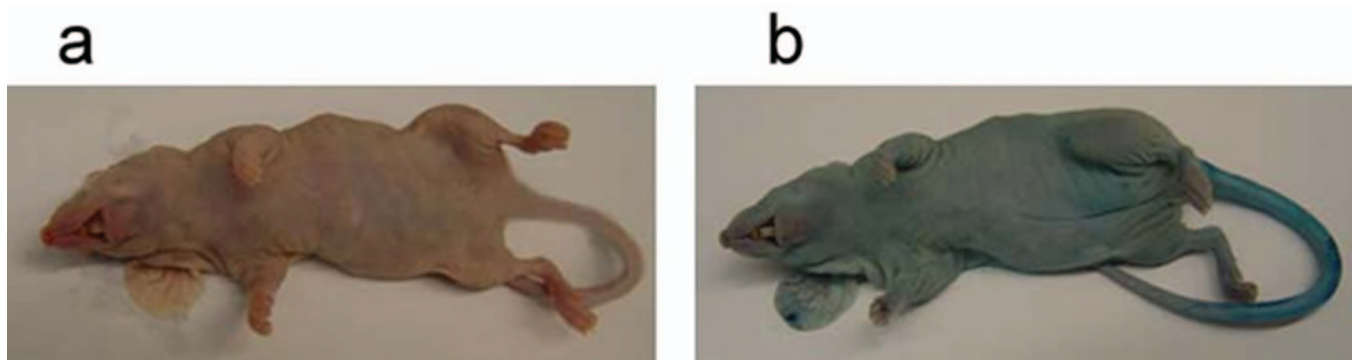


Fig. 4 Blue mouse: mouse under anesthesia (a) before and (b) after 15-min intravenous administration of Lymphazurin.

The laser beams in most of the experiments had a circular geometry with diameters comparable to vessel diameters (see Sec. 4.1.3 for details). In specific cases to distinguish closely located cells in flow, the laser beam was adjusted in a linear (elliptical) configuration approximately 6 μm wide with the use of an additional cylindrical lens and a slit. For the detection of rare cells, the beam diameter was expanded to preclude any missing cells because of the relatively low laser-pulse rates.

Navigation of the laser beams was controlled with a high-resolution (~ 300 nm) transmission digital microscopy (TDM) with a Cascade 650 charge-coupled device (CCD) camera (Photometrics, Roper Scientific, Inc., Trenton, New Jersey). A fluorescence module with colored CCD cameras (Nikon DXM1200) was added to the integrated system (Fig. 2) to verify PA/PT data using selected cells tagged with specific fluorescent labels.

A feasibility study was first performed *in vitro* with cells in suspension in conventional microscope slides. To model flow conditions, a flow module fitted with a syringe pump-driven system (KD Scientific, Inc., Holliston, Massachusetts) was used with glass microtubes of different diameters in the range of 30 to 150 μm to 1 to 4 mm.²⁶ This phantom provided flow velocities of 1 to 10 mm/sec, which are typical for blood flow in animal microvessels.²⁹

2.2 Animal Model

The feasibility studies of PAFC *in vivo* involved mouse (a nude) and rat (White Fisher, F344) models. Most experiments for PA detection of circulating cells were performed in thin (~ 270 μm), relatively transparent (i.e., also suitable for PTFC in transillumination mode) mice ear with well-distinguished blood microvessels [Figs. 3(a) and 3(b)]. The ear blood vessels examined were located 30 to 100 μm deep and had diameters in the range of 30 to 70 μm and blood velocities of 1 to 5 mm/sec. After standard anesthesia (ketamine/xylazine, 50/10 mg/kg), an animal was placed on the customized heated microscope stage, together with a topical application of warm water, which provided acoustic matching between the transducer and the ear. Some experiments were performed also with rat ear [Fig. 3(a)], which still had a distinguished blood microvessel in spite of its thicker structure compared to mice ear [Fig. 3(c)]. Selected experiments were performed with the rat mesentery [Fig. 3(d)], which has an almost ideal biostructure for PAFC *in vivo* because it consists of very thin (7 to 15 μm) transparent connective tissue with a single layer of blood and lymph microvessels [Fig. 3(d)]. For this procedure, the rat was anesthetized (ketamine/xylazine, 50/10 mg/kg), and the mesentery after exposure was placed on a heated (37.7°C) stage and bathed in warm Ringer's solution (37°C, pH 7.4).

2.3 Samples

The PAFC's capacity was estimated by intravenous injection of nanoparticles, contrast dyes, and bacteria into the animal tail vein. The gold nanoparticles such as GNRs and nanoshells (GNSs) were provided by the laboratory of Nanoscale Biosensors at the Institute of Biochemistry and Physiology of Plants and Microorganisms, Saratov, Russia. The GNRs were prepared using the seed-mediated growth method, as originally

developed by Jana, Gearheart, and Murphy³⁰ and Nikoobakht El-Sayed³¹ with minor modifications.³² Both "seed" and growth solutions included a cetyltrimethylammonium bromide (CTAB) surfactant. The silica/gold nanoparticles were prepared by the well-established two-step protocol.^{33,34} On the basis of TEM and the dynamic light scattering analyses, the geometrical parameters of nanoparticles were estimated to be of average diameter 15 nm and length 45 nm for GNRs, and average silica core diameter 60 nm and 20-nm gold coating (total diameter around 100 nm) for GNSs. For both sorts of particles, the concentration was about 10^{10} particles/ml. Two types of GNRs and GNSs were used in our experiments: 1. nanoparticles without surface modification, and 2. nanoparticles functionalized by thiol-modified polyethylene glycol (PEG) according to the established protocol.³⁵

Single-walled and multiwalled carbon nanotubes (CNT) were purchased from Carbon Nanotechnologies Incorporated (Houston, Texas) and Nano-Lab Incorporated (Newton, Massachusetts), respectively. The CNT samples used in this study were processed as described previously.^{36,37} The average length and diameter were 186 and 1.7 nm for the single-walled CNT, and 376 and 19.0 nm for the multiwalled CNT.

The bacterium *S. aureus* strain designated UAMS-1 was isolated from a patient with osteomyelitis at the McClellan Veterans Hospital in Little Rock, Arkansas.³⁸ The strain was deposited with the American Type Culture Collection and is available as strain ATCC 49230. UAMS-1 was cultured in tryptic soy broth and grown aerobically for 16 h at 37°C. Cells were harvested by centrifugation, resuspended in sterile phosphate buffered saline (PBS) and incubated with CNTs or ICG as follows. Before incubation, ICG was filtered through a 0.22- μm pore-size filter. Aliquot (150 μl) of bacteria in suspension was incubated with 150 μl (375 μg) of ICG solution for 30 min and 2 h at 37°C. Labeled bacteria were centrifuged (5000 rpm; 3 min) and the pellet was resuspended in PBS. Before incubation, the CNT solutions were further treated with interrupted ultrasound (US) for 10 min: 1.5 min of US (power 3 W) and 0.5 min of interruption. Aliquot (150 μl) of bacteria in suspension was incubated with 150 μl of CNT solution for 30 min and 2 h at room temperature. Labeled bacteria were centrifuged (10,000 rpm; 5 min) and the pellet was resuspended in PBS.

E. coli K12 strain was obtained from the American Type Culture Collection (Rockville, Maryland). *E. coli* was maintained in Luria-Bertani (LB) medium (1% tryptone; 0.5% yeast extract; 0.5% NaCl; pH 7). Aliquot (100 μl) of *E. coli* in PBS was incubated with 100 μl of the aforementioned CNT solution for 60 min at room temperature.

Indocyanine green (ICG) was purchased from Akorn Incorporated. Lymphazurin™ 1% (Isosulfan Blue) was manufactured by Ben Venue Labs Incorporated.

3 Results

3.1 Evaluation of Photoacoustic Flow Cytometry's Noninvasiveness

For noninvasive cell studies, the principal task was to evaluate the laser-induced damage threshold at the single cell level. We performed these important measurements using recently developed methodology, which assumes the specific changes in

Table 1 Photodamage threshold for single blood cells in near-IR spectral range.

Wavelength, nm		740	760	780	800	820	840	860	880	900	920	960
Photodamage threshold ED ₅₀ , J/cm ² (for 8 nsec pulse width)	Rat RBCs	6.9	6.8	17.7	17.5	28.0	43.5	43.8	76.5	69.4	77.7	33.5
	Rat WBCs	21.7		152	219	251		730			357	48.8

PT images and PT responses from individual cells as a function of the pump-laser energy.^{21,39} The method was verified with a conventional assay such as Trypan Blue exclusion. In agreement with the previous study,³⁹ for relatively strong absorbing RBCs in the visible spectral range, the photodamage threshold ED₅₀ (50% of cells damaged) *in vitro* varied in the range of 1.5 to 5 J/cm² with a laser wavelength in the range of 417 to 555 nm (for a 20- μ m laser spot). However, for other cells with lower absorption, the thresholds were higher: 12 to 42 J/cm² for lymphocytes and 36 to 90 J/cm² for K562 blast cells. In the NIR spectral range, where most cells have minimal absorption, the ED₅₀ damage thresholds were lower than those for wavelengths in the visible-spectral range. Specifically, the damage thresholds for RBCs and WBCs in the spectral range of 860 to 920 nm (Table 1) were more than 1 order magnitude less compared to those in the visible spectral range. The measurement of laser-induced cell damage *in vivo* using change in PT responses¹⁶ revealed that within the accuracy of experiments ($\sim 15\%$), the photodamage cell thresholds *in vitro* and *in vivo* were similar. A PAFC's noninvasiveness was achieved in most studies by choosing laser fluence much below the estimated cell photodamage threshold according to the laser safety standard of 34 mJ/cm² in the NIR spectral range for the condition of our experiments.⁴⁰

3.2 Photoacoustic Flow Cytometry's Parameter Verification with Conventional Contrast Agents

The capability of PAFC was estimated first with standard contrast vital dyes, which are widely used to study physiological function of blood and lymph system in normal or for disease diagnostics, such as cancer or cardiovascular and lymphatic disorders, among others.^{7,27} Specifically, in the current study we extended PAFC on the kinetic study of Lymphazurin, which was used before, mostly for the delineation of lymphatic vessels.^{41,42} Lymphazurin's exact pharmacological action and its kinetics in the blood circulation and surrounding tissue are still unclear.

An aqueous solution of Lymphazurin (200 μ l; 1% concentration) was injected into mouse and rat blood circulatory systems through the tail vein. The observed dynamic effects were very similar in both mice and rats. In particular, a few minutes after the injection, mouse tail, nose, and lips turned blue quickly with complete coloration of the whole skin body within 15 min [Fig. 4(b)]. For approximately 1 h, the animal's skin remained blue. Then, the animal's skin became lighter and returned to normal after ~ 3 h. After anesthesia ended, visual qualitative monitoring revealed no adverse effects, including no changes in vital signs and no differences in

the animal behavior compared to the control group with no dye injection. These findings are in line with the published data of low toxicity and safety regarding this dye at the doses used.⁴¹ Selected animals were sacrificed 3 h after injections and were anatomically examined. No organ accumulation of the dye was seen except the urine tract and biliary excretion, which is in agreement with other previously reported data.⁴¹ This study suggested extremely high permeability of dye through the blood vessel walls, followed by fast distribution into tissue.

Lymphazurin has a relatively flat absorption band in the spectral range of 570 to 660 nm with a sharp boundary (i.e., outside this range, the absorption quickly drops down). For PA detection, we have chosen the wavelength of 650 nm, where absorption of Lymphazurin is close to maximum, while the blood absorption drops down to the level which is almost 1 order magnitude less compared to maximum blood absorption near 580 nm.⁴³ The PA signals from blood vessels [e.g., 240 mV in Fig. 5(a)] were slightly higher than the PA background signals from surrounding tissue [e.g., 160 mV in Fig. 5(b)], i.e., approximately 1.5 times. The continuous monitoring of PA signals from the ear blood microvessels with average diameter 50 μ m after intravenous administration of Lymphazurin with the standard (1%) concentration in 200 μ l solution revealed fast (within a few minutes) Lymphazurin appearance in blood flow, followed by its clearance half-life of 30 min and total disappearance from the blood within approximately 50 min (Fig. 6). Maximum PA signals from the blood vessel after dye administration [Fig. 5(c)] were approximately three times higher than the PA signals from blood vessels before dye administration [Fig. 5(a)]. The PA signals from tissue around the vessels after dye injections [Fig. 5(d)] gradually increased 2 to 2.5 times during 15 to 20 min and then remained relatively constant for approximately 1 to 1.5 h. This level was comparable to or even a little higher than the background PA signals from blood vessels when Lymphazurin was cleared from the blood pool. The measurement of PA signals during the scanning laser beam across ear tissue revealed the readable increase in the PA signals in some local areas that can probably be associated with dye uptaken by lymphatics. We did not observe readable PA signal changes in amplitude and shape as precursors of photodamage phenomena³⁹ that suggest noninvasive condition for one pulse irradiation at used laser fluence in the range 30 mJ/cm², although this issue requires further verification.

3.3 Detection of Circulating Gold Nanoparticles

The 250- μ l suspension of GNRs in concentration of 10¹⁰/ml was injected to the rat blood circulation through the vein tail

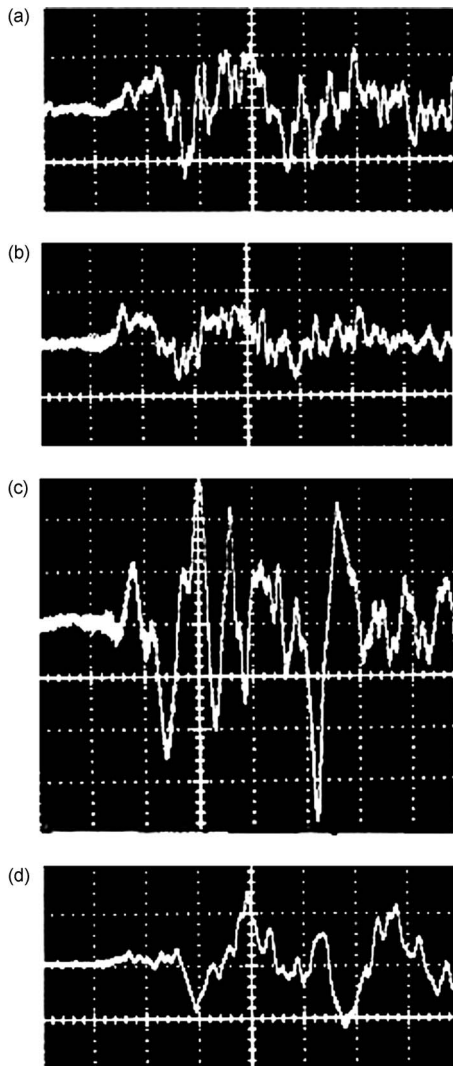


Fig. 5 PA signals from blood flow in (a) mouse ear vessel with diameter $\sim 50 \mu\text{m}$ and (b) from surrounding skin before dye injection. (c) PA signal from blood flow with Lymphazurin 5 min after injection (d) PA signal from skin 20-min after dye injection. Laser parameters: wavelength 650 nm, fluence $30 \text{ mJ}/\text{cm}^2$. Amplitude/time scale: (a), (b), and (c) $200 \text{ mV}/\text{div}/1 \mu\text{s}/\text{div}$, (d) $500 \text{ mV}/\text{div}/1 \mu\text{s}/\text{div}$.

followed by continuous monitoring of PA signals from blood vessels with $50 \mu\text{m}$ diameter in the rat mesentery. The chosen laser wavelength of 830 nm was close to the maximum absorption of GNRs. Uncoated GNRs were rapidly cleared from the blood circulation within 1 to 3 min preferentially by the reticuloendothelial system (RES). After PEGylated GNR injection, the fluctuated strong PA signals appeared with the amplitudes significantly exceeding the PA background signals from blood vessels approximately within the first minute and lasted from 14 to 25 min, depending on the individual animal (Fig. 7). Simultaneously, the slightly fluctuated PA background increased approximately 1.5 to 2 times above the background from blood at 3 min and lasted around 4 min. These measurements were performed in three animals, and the average data of the number of circulating GNRs per minute are shown in Fig. 8. In average, the maximum number of individual PA signals was achieved 3 to

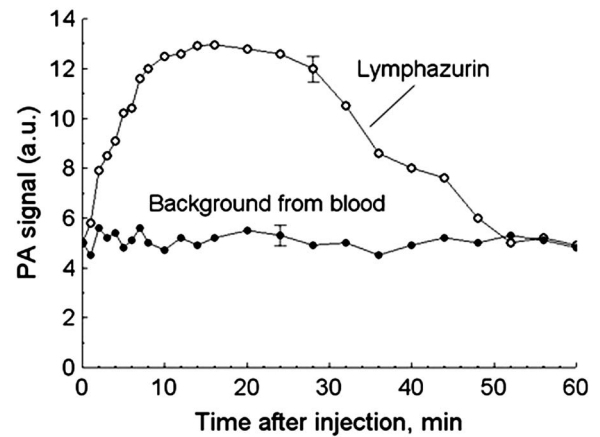


Fig. 6 Quantitative PA monitoring of Lymphazurin in blood flow of rat ear microvessel with diameter $50 \mu\text{m}$ after intravenous injection of dye in the tail vein. Laser parameters: wavelength 650 nm, fluence $30 \text{ mJ}/\text{cm}^2$, beam diameter $40 \mu\text{m}$.

5 min after injection, with gradual decrease in the rate of their appearance as time elapsed during 15 min. In one animal, during the clearance process, a relatively strong random fluctuation of the PA signals was observed. This can be associated with a nonoptimal tail injection when some GNRs could accumulate near the injected site and then enter into the vein vessels with some delay compared to the initial injection. The verification of these data is currently under investigation.

3.4 Detection of Single Circulating Bacteria

3.4.1 Detection of *Staphylococcus aureus*

The capability of PAFC to monitor circulating single *S. aureus* in blood flow was estimated with the mouse ear model. Because the endogenous absorption of bacteria was relatively weak compared to blood absorption even in the NIR spectral range, bacteria were labeled with NIR absorbing contrast agents such as ICG, GNRs, GNSs, and CNTs. The incubation of *S. aureus* with these agents was performed for 30 min and 2 h at 37°C without antibodies to avoid the potential influence of immunogenicity on bacteria circulation. Except CNTs, the other labeling agents showed slight toxicity at 2-h incubation. Hence, 30-min incubation was used in most experiments to avoid their potential cytotoxic effects. The labeling efficiency was estimated using methodology of the PT aggregation/clusterization assay.^{26,44} In particular, Fig. 9 shows the PT thermolens signals in the time-resolved mode (Sec. 2.2) from bacteria alone [Fig. 9(a)] and from bacteria labeled with ICG [Fig. 9(b)] and CNTs [Fig. 9(c)]. At relatively high laser fluence ($\sim 24 \text{ J}/\text{cm}^2$), which nevertheless was below the bacteria photodamage in the NIR spectral range used (795 nm), the classic linear PT response²¹ was observed for the control bacteria alone, as indicated by an initial peak due to fast laser-induced heating of the bacteria and a slower exponential tail corresponding to bacteria cooling through heat diffusion into the surrounding solution [Fig. 9(a)]. The high laser fluence required, and nevertheless, still relatively low PT and PA signal amplitudes [data not shown; similar to those in Fig. 5(b)] prevented us using bacteria without labeling for their detection *in vivo* in the background of

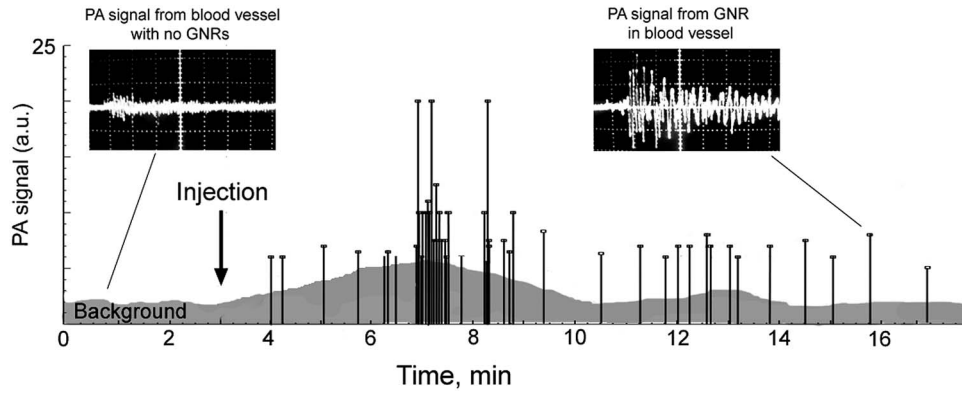


Fig. 7 PA signals from circulating GNRs in blood flow in the rat mesentery microvessel with diameter of 50 μm as a function of time postinjection. Laser parameters: wavelength 830 nm, laser fluence 100 mJ/cm^2 . The amplitude/time scale on oscilloscope signals is 100 $\text{mV}/\text{div}/4 \mu\text{s}/\text{div}$.

RBCs, because of the possible RBC damage and the influence of background absorption from blood. Staining *S. aureus* with ICG led to significant PA signal amplitude increase [Fig. 9(b)], on average almost 2 orders of magnitude. This allowed us to reduce the laser fluence to safety level 34 mJ/cm^2 .

Labeling *S. aureus* with CNTs and their clusters yielded more dramatic increase of PT signal amplitude, which was several times higher than that from bacteria with ICG at the same laser energy. The amplitude of the PT response rapidly increased with increases in the pulse energy, until the overheated local effects around CNTs clusters led to the bubble formation, which resulted in a negative peak [Fig. 9(c)] due to bubble-dependent changes in local temperature, refractive index, and light scattering phenomena.^{21,38} The degree of increase in PT signal amplitudes and bubble-associated effects were used to optimize the labeling procedure almost in real time with different nanoparticles. The best results were obtained with GNRs, but its toxicity related to the preparation procedure required further studies.²⁷ Minimal bacteria binding was obtained both with nonconjugated and PEGyted GNSs. Thus, for next experiments *in vivo*, we have chosen ICG and CNTs because of their relatively high labeling efficiency and low toxicity.

Labeled bacteria in suspension, with volumes of 100 μl and concentration of $5 \times 10^5/\text{ml}$, were injected into the

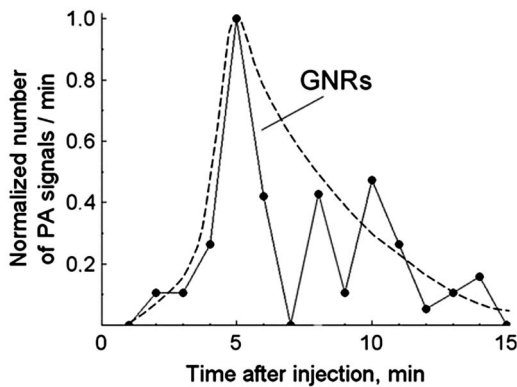


Fig. 8 Normalized number of circulating GNRs in blood microvessels of the rat mesentery as a function of time postinjection. Dashed curve shows an average data with three rats.

mouse's circulatory system through the tail vein, followed by clearance monitoring with the PAFC in mouse ear blood microvessels with an average diameter of 50 μm (Fig. 10). The obtained results were similar to both ICG and CNT contrast agents: the rapid appearance of bacteria in the ear blood microvessels after injection within the first minute, followed by their elimination from the blood circulation after 3 to 5 min. The periodical PA monitoring of mice blood vessels within a few days revealed that bacteria with CNTs kept appearing for more than 2 days with the average rate of one PA signal per 3 min. The complete clearance with no sign of circulating bacteria was observed 60 h after injections.

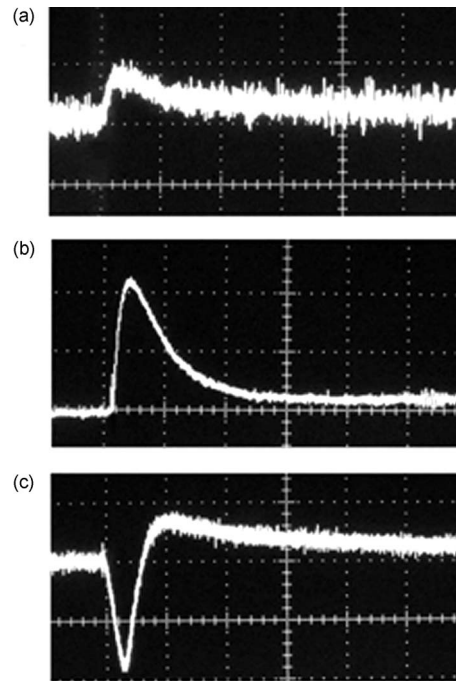


Fig. 9 PT signals from (a) *S. aureus* cluster, (b) *S. aureus* stained with ICG, and (c) *S. aureus* labeled with carbon nanotubes (CNTs). Amplitude/time scale (laser pump wavelength)/(laser fluence): (a) 10 $\text{mV}/\text{div}/1 \mu\text{s}/\text{div}/795 \text{ nm}/24 \text{ J}/\text{cm}^2$; (b) 100 $\text{mV}/\text{div}/1 \mu\text{s}/\text{div}/795 \text{ nm}/80 \text{ mJ}/\text{cm}^2$; and (c) 50 $\text{mV}/\text{div}/1 \mu\text{s}/\text{div}/850 \text{ nm}/24 \text{ mJ}/\text{cm}^2$.

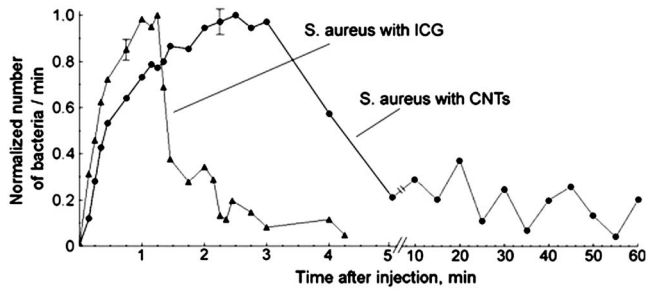


Fig. 10 Normalized number of circulating *S. aureus* in blood microvessels of mouse ear as a function of time postinjection, and label type (ICG and CNTs). Laser parameters: wavelength 795 and 850 nm, respectively. Laser fluence: 50 and 20 mJ/cm², respectively.

Laser fluence range in these particular experiments was in the range of 20 to 50 mJ/cm², which is much less than the damage threshold for RBCs at wavelengths of 790 to 850 nm (Table 1). However, multiple laser exposure to bacteria with CNTs at 50 mJ/cm² led to a gradual decrease (several percents) in PA signal amplitude from pulse to pulse that can be associated with strong absorption by CNTs, leading to thermal and bubble-related disintegration of CNT clusters.³⁷

3.4.2 Photoacoustic detection of *Escherichia coli* labeled with carbon nanotubes

The methodology similar to the aforementioned was also applied for real-time monitoring of *E. coli* labeled with CNTs. Figure 11(a) exemplifies TEM images of an *E. coli* before and after 0.5-h incubation with CNTs, which demonstrates the excellent binding efficiency of CNTs at the bacterial surface with formation of local CNT clusters. Furthermore, using the standard viability kits revealed that bacteria viability was not affected by CNTs.³⁷ The CNT clusters provided more effective heating, and thus generation of PT signals from individual bacteria which exceeded the background PA signals from the blood pool [Fig. 11(b), top and bottom oscilloscope signals, respectively]. Bacteria labeled with CNTs have been intravenously administered to mice through the tail vein and monitored through the CNT's intrinsic NIR absorption at the wavelength of 850 nm with PAFC. After fast appearance of the bacteria, their concentrations in the blood decreased almost exponentially within a half-life of 6 min [Fig. 11(b)]. The absence of bi- or multiexponential kinetics indicates that there was no significant temporary accumulation of bacteria in a specific area (e.g., vessel wall or liver) that could act as reversible reservoirs. After a few days, the experimental animals displayed normal behavior and no evidence of adverse effects from bacteria injections. Therefore, we deduce an ab-

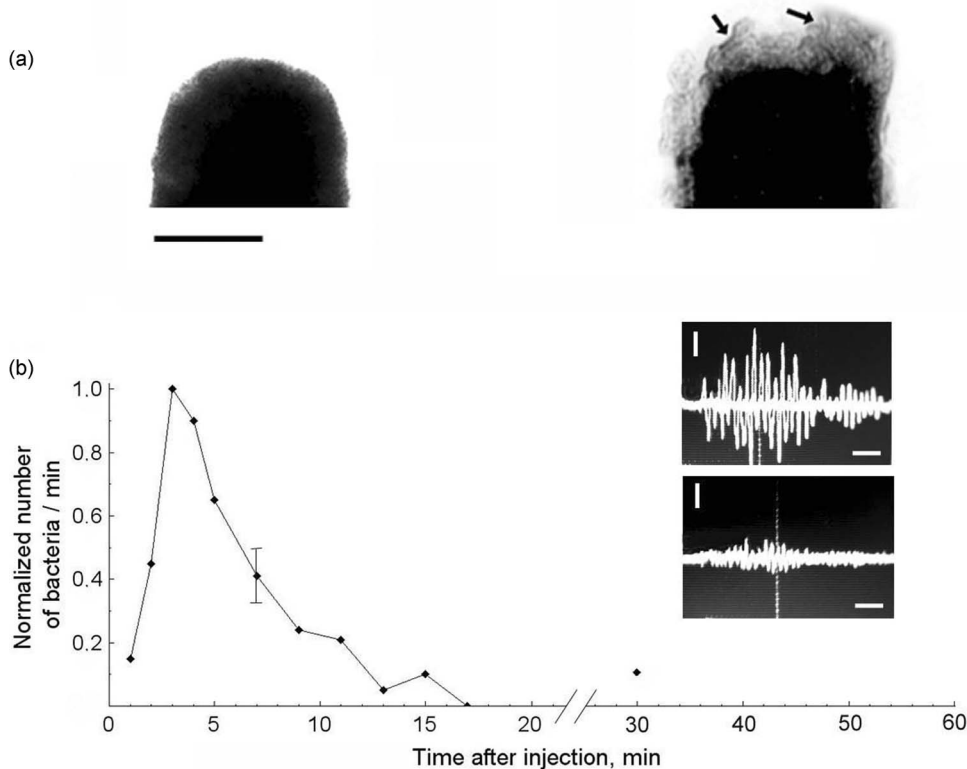


Fig. 11 (a) TEM images of an *E. coli* fragment before (left) and after (right) incubation with CNTs. Arrows indicate CNT clusters at the bacteria surface. Scale bars represent 500 nm. Normalized number of circulating *E. coli* in blood microvessels of mouse ear as a function of time postinjection. Oscilloscope signals: PA signals from labeled *E. coli* in blood (top) and from blood alone (bottom). Amplitude/time scale: 200 mV/div/2 μ s/div. Scale bar represents amplitude/time scale: 200 mV/div/2 μ s/div, respectively. Laser parameters: wavelength 850 nm, laser fluence 100 mJ/cm².

sence of acute toxicity for the dosage used here.

4 Discussion

This study demonstrates that the innovative combination of PA and FC techniques, each of which has been used for many years separately, may provide new opportunities for studying absorbing objects in the blood flow. We believe that the results presented in this work, together with our previous studies,^{27,28} show tremendous potential of PAFC for real-time monitoring of the depletion kinetics of circulating conventional contrast agents, blood and cancer cells, bacteria, and different nanoparticles in native biological environments *in vivo* in animal models. Considering that PAFC is a new tool in biological research, in this section, we discuss its technical features, its requirements in different applications, and further possible improvements on the basis of the obtained data.

4.1 Features of Photoacoustic Flow Cytometry

The detection of fast moving absorbing micro- or nano-objects of different origins on the background of the absorption of blood cells and surrounding tissue presents a new challenge for the PA technique. For noninvasive real-time detection of living cells or bacteria, most laser parameters are important, including wavelength λ , pulse duration t_p , pulse repetition rate f , and laser fluence Φ .

4.1.1 Laser pulse width

The cw lasers without amplitude (intensity) modulation are widely used in conventional *in vitro* FC to provide fluorescent or scattering detection methods.¹⁻³ The cw mode is not quite suited to PA methods in FC applications, because this mode does not provide an effective generation of PA signals, especially the s from small single objects.¹⁹ To enhance the PA signals, intensity modulation in the cw mode or pulse regime is required.¹⁵ To generate the maximum PA signal in the pulse mode with more efficient conversion of light energy into thermal, and then acoustic energy, the laser pulse duration t_p must meet thermal, and especially more strict acoustic (stress) confinement criteria,²² $t_p \leq \tau_A = 2R/c_s$, where τ_A is the transit time of the acoustic wave traveling through an absorbing object, R is the radius of the absorbing target, and c_s is the speed of sound in the object. For water, the parameter c_s is 1.5×10^5 cm/sec (for metals, several times higher). Thus, the pulse durations required for an object with diameter $D=2R$, ~ 5 to $15 \mu\text{m}$ (the typical cell sizes) and 0.5 to $1 \mu\text{m}$ (typical bacteria or cell organelle sizes) are $t_p \leq 7$ to 20 nsec and $t_p \leq 0.7$ to 1.4 nsec, respectively. Thus, the 8-ns pulse width used in this study is close to the optimum for detecting cells and bacteria, although smaller objects such as single nanoparticles in linear mode require shorter laser pulses (e.g., for 100-nm particles $\tau_A \approx 100$ ps). With nanosecond laser pulses, however, PA signals from nanoparticles can be enhanced through nonlinear phenomena as well as by clustering nanoparticles into cells or bacteria.^{37,38,44} Nanoparticle clusters of larger size and dense nanoparticle distribution may better meet the acoustic confinements. Therefore, the dependence of PA signals on nanocluster sizes may be used for real-time PA monitoring of nanoparticle clustering or aggregations. This new approach for PA nanocluster assays is currently under testing in our laboratory.

4.1.2 Laser pulse rate

To expose each fast flowing object, the laser must have a pulse repetition rate $f \geq (V_F)/D$, where V_F is the flow velocity.⁴⁵ For example, in small animal blood microvessels, typical flow velocity ranges from 1 mm/sec (capillary) to 10 mm/sec (arterioles),²⁹ and for $D=20 \mu\text{m}$, $f \geq 50$ to 500 Hz, respectively. To detect smaller objects, or at faster flow, the pulse repetition rate should be higher. The high rate is also essential to increase the PAFC sensitivity during multipulse object exposure, because the signal-to-noise ratio is proportional to the square root of the number of laser pulses. The multiexposure of the same cells should not be a problem at the laser noninvasiveness. A maximum data acquisition rate is presently limited by the 50-Hz laser pulse-repetition rate, which may lead to missing some fast circulating objects. Future work, which is now in progress, includes the use of lasers with higher pulse repetition rates such as diode and diode-pumped solid-state lasers as well as cw lasers with high frequency intensity modulation.

4.1.3 Laser beam diameter

In analogy to conventional FC, to distinguish closely located objects in flow, the minimum laser beam size should be comparable to or less than the object sizes (i.e., 1 to $10 \mu\text{m}$). The laser beams may have a circular geometry with diameters comparable to vessel diameters for the rare objects. However, for many of the closely located objects, the laser beam should be adjusted in a linear (elliptical) configuration (e.g., $6 \mu\text{m}$ wide and $55 \mu\text{m}$ long for this study). With the use of an elliptical beam shape with a long axis comparable to that of a vessel's diameter, the detection efficiency (i.e., the number of cells detected per the total number of cells passing through the vessels) is expected to be close to one in small blood vessels.

4.1.4 Laser safety

The laser fluence must meet the ANSI safety standard,⁴⁰ which is ~ 34 mJ/cm² in the NIR spectral region used in our experiments. At this low pulse energy fluence, high sensitivity of the developed acoustic detection system with a customized transducer and an optimized signal acquisition provided the reliable detection of PA signals from single labeled bacteria in the blood flow *in vivo* in the presence of electronic noise and background signals from normal blood cells and surrounding tissue. In addition, the cell-photodamage thresholds for RBCs were shown to be high in the NIR region (17 to 80 J/cm², Table 1). Thus, the high PA sensitivity, together with the high RBC damage thresholds at the NIR, provided PAFC noninvasiveness in the *in vivo* study.

4.1.5 Spectral range

The wavelength, which renders the maximum absorption contrast between labeled bacteria (or cancer cells)²⁷ and RBCs, lies in the NIR spectral range of 650 to 940 nm, depending on the optical properties of the PA labels (e.g., CNTs, GNSs, GNRs, and ICG). Possible spectral shifts of PA label absorption bands due to the interaction with blood components, labeling, aggregation, or clustering (e.g., as in the case of ICG or gold nanoparticles)^{7,8,44} should be taken into account. Thus, further verification is required to determine the optimal wavelength in each specific case in the presence of the background

signals from blood and surrounding tissues. In this study, for example, the PA signals from blood microvessels in mouse ear were approximately 1.5 to 2.5 times higher than the PA background signals from surrounding tissue in the spectral range of 650 to 850 nm. PA signals from thin unpigmented tissue, such as mesentery, were 3 to 4 times less compared to PA signals from thicker and more melanin pigmented ear tissue with bulk blood perfusion (i.e., capillary network). The real-time multispectral detection and identification of cells and bacteria in the blood circulation *in vivo* (as in modern multicolor FC *in vitro*) on the background of absorption by RBCs and surrounding tissue using multicolor PA labels should now be accomplished by the developed PAFC with extended spectral regions (420 to 2300 nm) and multibeam schematics.^{17,20,26–28}

4.1.6 Resolution and vessel depth

In this and previous studies,^{16,18,27} with focused laser beam schematics and spatial resolution of 10 to 30 μm , peripheral (dermal) vein, capillaries, arteries, and lymphatics with diameters of 10 to 150 μm were assessed using rat and mouse tissue at depths of 50 to 3000 μm . The attenuation of laser radiation in tissue is not critical in PAFC, because even after significant attenuation, the laser energy level is still sufficient to generate PA signals in deep vessels, which are detectable with highly sensitive PA schematics that take into account a low attenuation of acoustic waves in tissue.²² Besides, laser energy could be increased without yielding skin photodamage by skin surface cooling broadly used in laser medicine. Nevertheless, laser beam blooming due to scattering light may cause a decrease in the PAFC spatial resolution. It should not be too important in cases of detection of rare objects with large distances between them (100 μm or higher). However, to assess closely located moving objects in deep vessels, somewhat invasive approaches should be adopted, such as bypasses, and delivering light to vessels using fiber incorporated in tiny needles or catheters into the vessels.¹⁶ An alternative noninvasive approach is the time-resolved detection of PA signals from local vessel areas in combination with focused cylindrical high-frequency ultrasound transducers near the fiber or with the fiber into the transducer with the central hole. According to preliminary theoretical and experimental estimations, the expected resolutions are around 10 to 200 μm at depth up to a few centimeters, especially using PT/PA labels (e.g., gold nanorods).^{27,28}

4.2 Kinetics of Conventional Contrast Dyes

The conventional application of contrast dyes is based on their absorption or fluorescent properties, their good permeability, fast diffusion, and low toxicity. In particular, after administering some dyes (e.g., Evans Blue or Lymphazurin) the vessels can be easily identified visually with the naked eye because they are becoming darker compared to the surrounding tissue. The ability of PAFC to detect conventional agents was related to their limited quantum yield, typically in the range of 1 to 20%,⁶ resulting in transformations of the most absorbed energy into heat, to which the PA technique is very sensitive. Recent studies demonstrated the capability of ICG and Evans Blue dyes to enhance the PA image contrast of the blood vessels.^{46,47} However, most PA imaging algorithms cur-

rently in use for signal acquisition are not quite suitable for rapid real-time PA monitoring of contrast agent kinetics in fast blood circulation due to their time-consuming signal acquisition process (in most cases seconds, if not minutes). In addition, PA imaging still suffers from relatively poor spatial resolution (in the best case ≥ 50 to 100 μm),²² preventing its cytometric application at the single cell level. As described, the time-resolved PAFC with its high spatial (6 to 20 μm , see above, and 0.5 to 1 μm in imaging PT mode¹⁷), temporal (10^{-4} to 10^{-1} s, depending on the laser repetition pulse rate), and spectral (line width ≤ 0.5 nm) resolutions in the broad spectral range of 420 to 2300 nm has great potential for studying the kinetics of dyes with different absorption in the blood and lymph systems on different animals, including small mesentery models. We expect quick translation of this technology to humans, because some dyes (e.g., ICG) are already Federal Drug Administration (FDA) approved and lasers are used to meet the safety standard. PAFC should be applicable to monitor the kinetics of dyes simultaneously in blood flow, in tissue, and potentially in small lymphatics.¹⁸ The obtained data in this study strongly suggest the high possibility of extending the traditional fluorescent contrast agents as potential PA contrast agents. Furthermore, the combination of PAFC with such agents may extend PAFC's applicability. Detection of both fluorescent light and heat can increase the diagnostic value of integrated *in vivo* FC with PA and fluorescence detection techniques, especially far-red and NIR spectral ranges coinciding with the window transparency of specific tissue. It is important to note that the high absorption sensitivity of the PA technique made it possible to use relatively low concentrations of most dyes, especially with low quantum yields and a low laser energy levels, without notable signs of dye toxicity or photobleaching.

4.3 Detection of Single Nanoparticles In Vivo

Different nanoparticles are intensively being developed for biomedical applications, including diagnostics and therapy.^{33–36,44} Before any clinical application of nanoparticles can be feasible, it is imperative to determine critical *in vivo* parameters, namely pharmacological profiles, including the clearance half-time from the blood circulation.⁴⁸ In this study, we present previously unreported data on blood circulation of GNRs, which showed promise both as PA and PT labels and PT therapeutic agents for killing individual cancer cells and bacteria.^{27,49} In particular, the PEGylated GNRs remained for a longer time in the blood circulation after intravenous administration, compared to the nonPEGylated nanoparticles. Fast clearing of noncoated GNRs can be associated with quick GNR aggregation in blood flow immediately after intravenous injection, and the influence of the incompletely purified and partly toxic particle precursors, especially CTAB, which lead to fast responses of RES and the immune system.²⁷ It is known that PEG coating leads to reduced nanoparticle aggregations, protein binding, and adhesion to blood and endothelial cells.^{33,35} However, the observed clearance rate of around 15 min for the PEGylated GNRs was not as long as expected. It should be related to its nonoptimal preparation procedure, which leads to the presence of remaining toxic impurities or incomplete coating. Thus, the described technique should also be useful to the routine evaluation of the possible influence of

the natural properties of nanoparticles, the protective materials, and the coating procedures on their clearing. It should be noted that in the current study, the nonspecific binding and uncontrolled aggregation, which should be avoided for biomedical applications, were the subjects of discussion. Therefore, specific binding and aggregation (clustering) should be the next logical research to be conducted using additional bio-agents attached to the particles.⁴⁴

The detection threshold sensitivity of PAFC in this application can be estimated as follow. The 250- μl GNR suspension ($\sim 10^{10}/\text{ml}$) was injected in the blood pool of a rat with total blood volume of 25 ml. Assuming the ideal condition with no loss of GNRs during injection and circulation, the average GNR concentration in the rat blood pool should be $10^8/\text{ml}$. The irradiated (detected) volume in blood vessels is limited by a laser beam diameter of 25 μm and path length of around 45 μm across the vessel (i.e., comparable with vessel diameter), which gives the volume around $2.2 \times 10^{-8} \text{ cm}^3$. These parameters correspond to the estimated maximum number of GNRs in the detected volume around 2 to 3. The possible loss of GNRs during injections, such as adhesion in blood vessels and elimination by RES, may decrease this value several times, especially at the end of the elimination process. This strongly implies that the number of GNRs in the detection volume should be close to 1. Therefore, each pulse in Fig. 7 may be associated with the PA signals from individual GNRs. However, immediately after injection, local concentration of GNRs in the blood flow before redistribution in larger volume should be higher (i.e., many GNRs in the detected volume). This was confirmed by the increases in both individual PA signal rates and average PA background above the blood background in approximately 4 to 9 min (Fig. 7). In addition, in this time period, the PA signals with larger amplitudes were observed after each laser pulse. Essentially, these fluctuations were not accompanied by decrease of PA signal amplitude to zero, supporting the hypothesis of random appearance of several GNRs in the detected volume at the same time. This is similar to the aforementioned PA monitoring of Lymphazurin, when relatively large amounts of homogeneously distributed absorbing molecules appear in the detected volume, thus providing relatively stable continuous (i.e., not fluctuated) PA signals. On the contrary, only rare PA signals appeared even after many pulses at 10 min, suggesting the observation of the GNR clearance.

Laser fluence used in this study was of 100 mJ/cm^2 , which is at least 2 orders of magnitude less than the damage threshold for RBCs at the wavelength of 830 nm (Table 1). However, a recent study has suggested that high absorption of noble metal nanoparticles may lead to laser-induced nanoparticle modification, including their melting, evaporation, and explosion, accompanied by enhanced bubble and shock wave formation, even at relatively low laser fluence.⁵⁰ These nonlinear effects can lead to strong enhancement of PA signals from single gold nanoparticles due to the aforementioned highly localized shock wave and bubble formation, which may further increase PAFC sensitivity by the cost of the minimal invasiveness of the PA measurement at the current experimental conditions. The estimated PAFC sensitivity in the linear mode at lower laser energy is at least 3 to 5 gold nanoparticles in the detected volume. We also observed some

additional PA signal enhancement for PEG-coated gold nanoparticles due to the change in their thermal properties and their average size increase (up to 50 to 100 nm), leading to more effective nanoparticle heating and PA signal formation. This effect was more profound for GNSs due to probably more effective explosion of thin gold layers around a relatively large silica core (we called it the spherical piston explosion model). In addition, these effects might be important to increase the efficiency of PT nanotherapy with nanoparticles and their clusters used as a PT sensitizer for cancer cells or bacteria.⁵¹

The results obtained so far demonstrate unprecedented high sensitivity of the developed PAFC schematics, enabling single gold nanoparticle detection in blood flow *in vivo*. It also suggests the possibility of using a limited number of gold nanoparticles (e.g., 10 to 30) for cell labeling to achieve reliable PA detection of cells in the blood circulation.²⁷ In addition, the routine monitoring of the clearance rate of different nanoparticles may be combined with simultaneous real-time PA monitoring of nanoparticle accumulation in different organs in normal and pathological states (e.g., in tumors, lymph nodes, or infected areas).

4.4 Real-Time Detection of Single Circulating Bacteria In Vivo

Despite major advances in medicine in the last decade, micro-biologically based diseases continue to present enormous global health problems, especially due to the appearance of multidrug-resistant bacteria strains. The critical steps in the development of bacterial infections include their penetrations into the blood and lymph system, their interactions with blood cells in flow or with endothelial cells, and their toxin translocations in the host organisms.⁵² Increasing evidence has implicated the bacterial haematological and lymphatic translocation as the main sources for the induction of sepsis. Surprisingly, little is known about bacteria circulation in the blood pool, its clearance and adherence rates, and other kinetic parameters, which might be very important for understanding the transition from the bacteremic stage to the tissue-invasive stage of disease to develop effective therapies of infections.

In the current study, CNTs demonstrated great potential for labeling bacteria such as *S. aureus* and *E. coli* for FC diagnostics. High CNT binding efficiency may eliminate the bio-conjugation steps with biological recognition components, such as antibodies. This alleviates the potential influence of the additional biocomponents on clearance rates. Besides binding efficiency, the advantage of CNTs as contrast agents is their natural strong absorption in the NIR spectra. Therefore, compared to gold nanoparticles such as GNRs or GNSs, which require time-consuming preparation procedures, CNT itself does not need to be modified in any way to make it responsive to the NIR laser irradiation. Thus, the intrinsic NIR label absorption allows unambiguous observation of unmodified nanoparticles *in vivo*. To the best of our knowledge, the results from this study demonstrate for the first time that CNTs serve as excellent NIR high-contrast agents for PT and PA diagnostics, in addition to the previous reports showing their potential as high contrast PT sensitizer for cancer⁵³ and antimicrobial therapy.³⁷

The clearance of bacteria with CNTs was a little slower than that with ICG (Fig. 10), which can be explained by a slight ICG toxicity and more effective RES response, on the one hand, or by more effective bacteria labeling with CNTs (i.e., the presence of more labeled bacteria in the blood) on the other hand. The observed advantage of CNTs as a PT label compared to ICG (Fig. 9) can be explained by the stronger absorption of individual CNTs, and especially by CNT clusters, compared to ICG absorption.^{21,33,49} However, the absorption band of ICG is more narrow and specific compared to the not quite selective absorption of CNTs. Thus, besides binding efficiency, the choice of nanoparticles and dyes may depend also on requirements to selectivity. We plan also to use nanoscale liposomes filled up by ICG to increase the ICG local absorption as well as liposomes filled with CNTs and gold nanoparticles. However, such strong absorption may lead to the appearance of nonlinear phenomena, thus decreasing the labeled bacteria (and cell)²⁷ damage threshold. This implies that laser energy should be carefully selected to minimize such effects, although this should not be a problem during a single exposure of circulating bacteria with CNTs in blood flow.

The ultrasensitive, rapid PA detection of infection at a single bacteria level may supplement or replace conventional assays, for example, the time-consuming polymerase chain reaction (PCR) and others that are available currently *in vitro* only. The described PA technique is capable of detecting approximately 10^2 bacteria in the peripheral circulation of the small animal, such as mice and rats every ~ 15 min, with the potential to improve this parameter to ten bacteria. Theoretically, this technique enables us to detect just a single circulating cell or bacteria in the whole mice blood pool during continuous PA monitoring in the relatively large vessels approximately every hour. The obtained clearance rate for *S. aureus* (3 to 5 min) is in line with data obtained with fluorescent-labeled bacteria monitored with the dorsal skinfold chamber technique.⁵² However, the time-resolved PAFC revealed the fluctuation of clearance rates (Fig. 10). There are two possible explanations for the nature of these observations. First, this may be related to the bacterial adherence to endothelial cells, followed by bacteria extravasations in different organs, which are considered to play a central role in the invasive disease stage.⁵¹ Indeed, the scanning of the laser beam along vessels revealed the appearance of strong PA signals at different locations, indicating the adherence of bacteria with CNTs along the vessel wall. The adherence might be a dynamic process and can lead to periodical detachment of bacteria from blood vessel walls. We assume that the adherence can be influenced by bacteria labeling, especially with CNTs, which may prevent effective interaction of bacteria with other cells due to their high-density clustering on bacteria surfaces. Additionally, one cannot exclude the possibility of partial CNT detachment, especially in the relatively large CNT clusters, from bacteria surfaces during their interactions with other cells in fast blood flow. The detached CNTs could circulate longer than bacteria themselves, at least a few hours. In addition similar to the GNRs, the developed PAFC prototype demonstrated extremely high sensitivity in detecting individual CNTs and especially their small clusters. However, this topic is outside the scope of this work.

The scanning of the focused laser beam across ear tissue surrounding the examined blood vessels (PA mapping) revealed the strong local PA signals that can be associated with the presence of labeled bacteria in interstitium. This technique *in vivo* and *ex vivo* also revealed strong PA signals in liver (e.g., 24 h after administration), indicating the accumulation of bacteria in this organ. Additional studies are desired to elucidate the behavior of CNT-coated bacterial cells, as well as to optimize the processes of labeling bacteria with CNTs.

Compared to recent experiments with fluorescent or radioactive tracers with periodic examination of blood samples *in vitro*,^{48,52} we are confident that our time-resolved PA method with continuous monitoring *in vivo* is better suited for studying clearance rates of bacteria, as well as conventional and novel contrast agents, especially when elimination time is very short, a few minutes if not seconds.

5 Conclusion

The results in this study strongly suggest the excellent potential of PAFC as a new promising tool in biological research. This technology provides an unprecedented capability for real-time detection of circulating bacteria (and cells)²⁷ with ultra-high sensitivity as one bacteria (or cancer cell) in the background of 10^8 normal blood cells. This is unachievable with existing techniques, including advanced PCR and immunochimistry assays, even *in vitro* with cell enrichment. An analogy to standard *in vitro* FC, the PAFC may have a broad spectrum of similar applications *in vivo*, as well as provide many new applications that may include detection of various targets with intrinsic absorption or with PA labels targeting specific antigens and receptors (e.g., normal and abnormal cells, bacteria,^{37,38} viruses,⁴⁴ conventional contrast agents, and advanced nanoparticles) in a variety of vessels (e.g., arterioles, capillaries, veins, and afferent and efferent lymphatics) in assorted locations (e.g., skin, ear, mesentery, liver, and lymph nodes) for many disease models (e.g., cancer, infections, inflammation, and immune system disorders) and their combinations.

Further development of the presented work may solve very complex and largely unexplored areas of medicine related to detection of infections and stem, dendritic, and metastatic cells in different functional states (e.g., apoptosis) in lymph and blood flow at the single cell level. Especially, it may be used for early diagnostics of infection during hematogenous spread with bacteria translocation into different organs, vascular grafts, and stents. In particular, these infections commonly result in death at sepsis, despite aggressive treatment at the developed disease stage. A quick transition of this technology to humans is anticipated with the development of portable devices attached to the wrist or lymph nodes for alarm control of bacterial infection dissemination, cancer recurrence, metastasis development, therapy assessment (through controlling the number of circulating bacteria or metastatic cells), or monitoring of circulating drugs using nanoparticle-based drug carries (e.g., liposomes). PAFC technology may allow us to develop portable "personal" flow cytometers for blood testing without a needle stick using compact robust, low-cost, laser diode arrays with different wavelengths.

Acknowledgments

This work was performed at the University of Arkansas for Medical Sciences with support from the National Institutes of Health (NIH)/NIBIB under grant EB001858, EB00873, and EB005123 (Zharov), the National Research Initiative (NRI) of the USDA-CSREES grant 2005-35603-15902 (Kim), and the Arkansas Biosciences Institute (ABI) (Zharov and Kim). Khlebtsov, who provided GNRs and GNSs for this study, was supported by grants from the Russian Foundation for Basic Research (numbers 05-02-16776a and 07-02-01434-a) and the Ministry of Science and Education of the Russian Federation (numbers 02.513.11.3043 and 02.512.11.2034). The authors thank Mark Smeltzer for providing *S. aureus* and its labeling, Gal Safirstein for help with the mouse model, Scott Ferguson for his assistance with developing the heated stage and laser measurements, Nalinikanth Kotagiri for preparing CNT samples, and David Sliney for his consult on laser safety standards.

References

- H. Hogan, "Flow cytometry moves ahead," *Biophotonics Int.* **13**, 38–42 (2006).
- H. M. Shapiro, *Practical Flow Cytometry*, 3rd ed., Wiley-Liss, New York (1995).
- A. Moldavan, "Photoelectric technique for the counting of microscopical cells," *Science* **80**, 188–189 (1934).
- B. Molnar, F. Sipos, O. Galamb, and Z. Tulassay, "Molecular detection of circulating cancer cells. Role in diagnosis, prognosis and follow-up of cancer patients," *Dig. Dis.* **21**, 320–325 (2003).
- A. Chung, S. Karlan, E. Lindsley, S. Wachsmann-Hogiu, and D. L. Farkas, "In vivo cytometry: a spectrum of possibilities," *Cytometry* **69**, 142–146 (2006).
- J. Novak, I. Georgakoudi, X. Wei, A. Prossin, and C. P. Lin, "In vivo flow cytometer for real-time detection and quantification of circulating cells," *Opt. Lett.* **29**, 77–79 (2004).
- D. J. Bornhop, C. H. Contag, K. Licha, and C. J. Murphy, "Advances in contrast agents, reporters, and detection," *J. Biomed. Opt.* **6**(2), 106–110 (2001).
- X. Wei, J. M. Runnels, and C. P. Lin, "Selective uptake of indocyanine green by reticulocytes in circulation," *Invest. Ophthalmol. Visual Sci.* **44**, 4489–4496 (2003) (and references there).
- M. A. Nolte, G. Kraal, and R. E. Mebius, "Effects of fluorescent and nonfluorescent tracing methods on lymphocyte migration in vivo," *Cytometry* **61**, 35–44 (2004).
- J. L. Zhang, S. Yokoyama, and T. Ohhashi, "Inhibitory effects of fluorescein isothiocyanate photoactivation on lymphatic pump activity," *Microvasc. Res.* **54**, 99–107 (1997).
- J. Molnar, S. Petofi, T. Kurihara, H. Sakagami, and N. Motohashi, "Antiplasmodium and carcinogenic molecular orbitals of benz[c]acridine and related compounds," *Anticancer Res.* **13**, 263–266 (1993).
- E. R. Nestmann, G. R. Douglas, T. I. Matula, C. E. Grant, and D. J. Kowbel, "Mutagenic activity of rhodamine dyes and their impurities as detected by mutation induction in Salmonella and DNA damage in Chinese hamster ovary cells," *Cancer Res.* **39**, 4412–4417 (1979).
- D. A. Berk, M. A. Swartz, A. J. Leu, and R. K. Jain, "Transport in lymphatic capillaries. 2. Microscopic velocity measurement with fluorescence photobleaching," *Am. J. Physiol.* **39**, H330–337 (1996).
- V. Zharov, E. Galanzha, and V. Tuchin, "Photothermal imaging of moving cells in lymph and blood flow in vivo animal model," *Proc. SPIE* **5320**, 256–263 (2004).
- V. P. Zharov, E. I. Galanzha, and V. V. Tuchin, "Photothermal image flow cytometry in vivo," *Opt. Lett.* **30**, 628–630 (2005).
- V. P. Zharov, E. I. Galanzha, and V. V. Tuchin, "Integrated photothermal flow cytometry in vivo," *J. Biomed. Opt.* **10**, 51502 (2005).
- V. P. Zharov, E. I. Galanzha, and V. V. Tuchin, "In vivo photothermal flow cytometry: imaging and detection of cells in blood and lymph flow (review/prospect)," *J. Cell. Biochem.* **97**, 916–932 (2006).
- E. I. Galanzha, V. V. Tuchin, and V. P. Zharov, "Advances in small animal mesentery models for in vivo flow cytometry, dynamic microscopy, and drug screening (review)," *World J. Gastroenterol.* **14**, 192–218 (2007).
- V. P. Zharov and V. S. Letokhov, *Laser Optoacoustic Spectroscopy*, Springer-Verlag, Berlin (1986).
- V. P. Zharov, "Laser optoacoustic spectroscopy in chromatography," in *Laser Analytical Spectrochemistry*, V. S. Letokhov, Ed., pp. 229–271, Mass: Bristol, Boston (1986).
- V. P. Zharov and D. O. Lapotko, "Photothermal imaging of nanoparticles and cells (review)," *IEEE J. Sel. Top. Quantum Electron.* **11**, 733–751 (2005).
- M. Xu and L. V. Wang, "Photoacoustic imaging in biomedicine," *Rev. Sci. Instrum.* **77**, 041101 (2006).
- V. P. Zharov, E. I. Galanzha, and V. V. Tuchin, "Confocal photothermal flow cytometry in vivo," *Proc. SPIE* **5697**, 167–176 (2005).
- V. P. Zharov, M. Viegas, and L. Soderberg, "Biological detection of low radiation doses with integrated photothermal assay," *Proc. SPIE* **5697**, 271–281 (2005).
- S. I. Kudryashov, S. D. Allen, E. I. Galanzha, E. Galitovskaya, and V. P. Zharov, "Photoacoustics of individual live cells and particles," *Proc. SPIE* **6086**, 60860J (2006).
- V. P. Zharov, E. I. Galanzha, and V. V. Tuchin, "Photothermal flow cytometry in vitro for detection and imaging of individual moving live cells (review)," *Cytometry* **71A**, 191–206 (2007).
- V. P. Zharov, E. I. Galanzha, E. V. Shashkov, N. G. Khlebtsov, and V. V. Tuchin, "In vivo photoacoustic flow cytometry for monitoring of circulating single cancer cells and contrast agents," *Opt. Lett.* **31**, 3623–3625 (2006).
- V. Zharov, E. Galanzha, E. Shashkov, N. Khlebtsov, and V. Tuchin, "In vivo photoacoustic flow cytometry for real-time monitoring of circulating cells and nanoparticles," *SPIE News Room*, 0.1117/2.1200609.0391 (2006).
- S. E. Charm and G. S. Kurland, *Blood Flow and Microcirculation*, Wiley and Sons, New York (1974).
- N. R. Jana, L. Gearheart, and C. J. Murphy, "Wet chemical synthesis of high aspect ratio cylindrical gold nanorods," *J. Phys. Chem.* **105**, 4065–4067 (2001).
- B. Nikoobakht and M. A. El-Sayed, "Preparation and growth mechanism of gold nanorods using seed-mediated growth method," *Chem. Mater.* **15**, 1957–1962 (2003).
- A. V. Alekseeva, V. A. Bogatyrev, L. A. Dykman, B. N. Khlebtsov, L. A. Trachuk, A. G. Melnikov, and N. G. Khlebtsov, "Preparation and optical scattering characterization of Au nanorods, and their application to a dot-immunogold assay," *Appl. Opt.* **44**, 6285–6295 (2005).
- L. R. Hirsch, A. M. Gobin, A. R. Lowery, F. Tam, R. A. Drezek, N. J. Halas, and J. L. West, "Metal nanoshells," *Ann. Biomed. Eng.* **34**, 15–22 (2006).
- B. N. Khlebtsov, V. A. Bogatyrev, L. A. Dykman, and N. G. Khlebtsov, "Spectra of resonance light scattering of gold nanoshells: Effects of polydispersity and limited electron free path," *Opt. Spectrosc.* **102**, 233–241 (2007).
- H. Liao and J. H. Hafner, "Gold nanorod bioconjugates," *Chem. Mater.* **17**, 4636–4641 (2005).
- J.-W. Kim, N. Kotagiri, J. H. Kim, and R. Deaton, "In situ fluorescence microscopy visualization and characterization of nanometer-scale carbon nanotubes labeled with 1-pyrenebutanoic acid, succinimidyl ester," *Appl. Phys. Lett.* **88**, 213110 (2006).
- J.-W. Kim, E. V. Shashkov, E. I. Galanzha, N. Kotagiri, and V. P. Zharov, "Photothermal antimicrobial nanotherapy and nanodiagnostics with self-assembling carbon nanotube clusters," *Lasers Surg. Med.* **39**, 622–634 (2007).
- V. P. Zharov, K. E. Mercer, E. N. Galitovskaya, and M. S. Smeltzer, "Photothermal nanotherapeutics and nanodiagnostics for selective killing of bacteria targeted with gold nanoparticles," *Biophys. J.* **90**, 619–627 (2006).
- D. O. Lapotko and V. P. Zharov, "Spectral evaluation of laser-induced cell damage with photothermal microscopy," *Lasers Surg. Med.* **36**, 22–33 (2005).
- "American National Standard for Safe Use of Lasers," ANSI Z136.1 (2000).

41. J. I. Hirsch, J. Tisnado, S. R. Cho, and M. C. Beachley, "Use of Isosulfan blue for identification of lymphatic vessels: Experimental and clinical evaluation," *AJR, Am. J. Roentgenol.* **139**, 1061–1064 (1982).
42. L. L. Burgoyne, D. W. Jay, G. B. Bikhazi, and A. J. De Armendi, "Isosulfan blue causes factitious methemoglobinemia in an infant," *Paediatr. Anaesth.* **15**, 1116–1119 (2005).
43. A. Roggan, M. Friebel, K. Dorschel, H. Andreas, and G. Muller, "Optical properties of circulating human blood in the wavelength range 400–2500 nm," *J. Biomed. Opt.* **4**(1), 36–46 (1999).
44. V. P. Zharov, J.-W. Kim, M. Everts, and D. T. Curiel, "Self-assembling nanoclusters in living systems: application for integrated photothermal nanodiagnostics and nanotherapy (review)," *Nanomedicine* **1**, 326–345 (2005).
45. V. P. Zharov, E. I. Galanzha, Y. A. Menyayev, and V. V. Tuchin, "In vivo high-speed imaging of individual cells in fast blood flow," *J. Biomed. Opt.* **11**, 054034 (2006).
46. M. C. Pilatou, E. Marani, F. F. de Mul, and W. Steenbergen, "Photoacoustic imaging of brain perfusion on albino rats by using Evans blue as contrast agent," *Arch. Physiol. Biochem.* **111**, 389–97 (2003).
47. X. Wang, G. Ku, M. A. Wegiel, D. J. Bornhop, G. Stoica, and L. V. Wang, "Noninvasive photoacoustic angiography of animal brains in vivo with near-infrared light and an optical contrast agent," *Opt. Lett.* **29**, 730–732 (2004).
48. P. Cherukuri, C. J. Gannon, T. K. Leeuw, H. K. Schmidt, R. E. Smalley, S. A. Curley, and R. B. Weisman, "Mammalian pharmacokinetics of carbon nanotubes using intrinsic near-infrared fluorescence," *Proc. Natl. Acad. Sci. U.S.A.* **103**, 18882–18886 (2006).
49. X. Huang, I. H. El-Sayed, W. Qian, and M. A. El-Sayed, "Cancer cell imaging and photothermal therapy in the near-infrared region by using gold nanorods," *J. Am. Chem. Soc.* **128**, 2115–2120 (2006).
50. R. R. Letfullin, C. Joenathan, T. F. George, and V. P. Zharov, "Laser-induced explosion of gold nanoparticles: Potential role for nanophotothermolysis of cancer," *Nanomedicine* **1**, 473–480 (2006).
51. V. Zharov, E. Galanzha, E. Shashkov, I. Maksimova, B. Khlebtsov, N. Khlebsov, G. Terentuk, G. Akchurin, and V. Tuchin, "In vivo detection and killing of individual circulating metastatic cells," *Lasers Surg. Med.* **19** Suppl., 47 (2007).
52. M. W. Laschke, S. Kerdudou, M. Herrmann, and M. D. Menger, "Intravital fluorescence microscopy: a novel tool for the study of the interaction of *Staphylococcus aureus* with the microvascular endothelium in vivo," *J. Infect. Dis.* **191**, 435–443 (2005).
53. N. W. Kam, M. O'Connell, J. A. Wisdom, and H. Dai, "Carbon nanotubes as multifunctional biological transporters and near-infrared agents for selective cancer cell destruction," *Proc. Natl. Acad. Sci. U.S.A.* **102**, 11600–11605 (2005).